The scattering of the harmonic anti-plane shear stress waves by two collinear interface cracks between two dissimilar functionally graded piezoelectric/piezomagnetic material half-infinite planes dynamic loading

Z-G Zhou[1]* and **B Wang**[2]

[1]Center for Composite Materials, Harbin Institute of Technology, Harbin, People's Republic of China
[2]School of Physics and Engineering, Sun Yat-Sen University, Guangzhou, People's Republic of China

The manuscript was received on 17 July 2005 and was accepted after revision for publication on 18 November 2005.

DOI: 10.1243/09544062JMES129

Abstract: In this paper, the dynamic behaviour of two collinear interface cracks between two dissimilar functionally graded piezoelectric/piezomagnetic material half-infinite planes subjected to the harmonic anti-plane shear stress waves is investigated. To make the analysis tractable, it is assumed that the material properties vary exponentially with coordinate vertical to the crack. By using the Fourier transform technique, the problem can be solved with the help of a pair of triple integral equations, in which the unknown variable is the jump of the displacements across the crack surfaces. These equations are solved by using the Schmidt method. The relations among the electric field, the magnetic flux field, and the dynamic stress field near the crack tips can be obtained. Numerical examples are provided to show the effect of the functionally graded parameter, the distance between two interface cracks, and the circular frequency of the incident waves upon the stress, the electric displacement, and the magnetic flux intensity factors of cracks.

Keywords: functionally graded piezoelectric/piezomagnetic materials, two collinear interface cracks, stress wave

1 INTRODUCTION

The piezoelectric/piezomagnetic composite materials have been found to have wide applications in the smart systems of aerospace, automotive, medical, and electric fields because of the intrinsic coupling characteristics among their electric, magnetic, and mechanical fields. As the piezoelectric/piezomagnetic composite materials are being extensively used as actuators or transducers in the technologies of smart and adaptive systems, the mechanical reliability and durability of these materials become increasingly important. Therefore, it is of great importance to study the magneto-electro-elastic interaction and fracture behaviours of magneto-electro-elastic composites [**1**–**12**]. On the other hand, the development of functionally graded materials has demonstrated that they have the potential to reduce the stress concentration and increase of fracture toughness. Consequently, some applications of functionally graded piezoelectric materials have been made [**13**, **14**]. Recently, the fracture problems of functionally graded piezoelectric materials have been considered in references [**15**–**20**]. Li and Weng [**19**] first considered the static anti-plane problem of a finite crack in functionally graded piezoelectric material strip. Their results showed that the singular stress and the singular electric displacement in functionally graded piezoelectric materials carry the same forms as those in the homogeneous piezoelectric materials

Corresponding author: Center of Composite Materials, Harbin Institute of Technology, PO Box 1247, Harbin, Hei-Long Jiang 150001, People's Republic of China. email: zhouzhg@hit.edu.cn

but the magnitudes of the intensity factors depend significantly upon the gradient of the functionally graded piezoelectric materials properties. More recently, the concept of functionally graded materials was first extended to the piezoelectric/piezomagnetic materials to improve the reliability of piezoelectric/piezomagnetic materials and structures in references [**21**, **22**]. The results also showed that the singular stress, the singular electric displacement, and the singular magnetic flux in functionally graded piezoelectric/piezomagnetic materials carry the same forms as those in the homogeneous piezoelectric/piezomagnetic materials but the magnitudes of the intensity factors depend significantly upon the gradient of the functionally graded piezoelectric/piezomagnetic materials properties. However, to our knowledge, the dynamic magneto-electro-elastic behaviour of functionally graded piezoelectric/piezomagnetic materials with two collinear interface cracks subjected to the harmonic anti-plane shear stress waves has not been studied. Thus, the present work is an attempt to fill this information needed. Here, we just attempt to give a theoretical solution for this problem.

In this paper, the dynamic magneto-electro-elastic behaviour of two collinear permeable interface cracks between two dissimilar functionally graded piezoelectric/piezomagnetic material half-infinite planes subjected to the harmonic anti-plane shear stress waves is investigated using the Schmidt method [**23**]. The advantages of the Schmidt method are that it can be used to solve the first kind Fredholm integral equation as shown in reference [**23**] and the special kind dual integral equations as discussed in reference [**24**]. To make the analysis tractable, it is assumed that the material properties vary exponentially with coordinate vertical to the crack. Fourier transform is applied and a mixed boundary-value problem is reduced to a pair of triple integral equations. To solve the triple integral equations, the jump of the displacements across the crack surfaces is expanded in a series of Jacobi polynomials. Numerical solutions are obtained for the dynamic stress, the electric displacement, and the magnetic flux intensity factors for permeable crack surface conditions.

2 FORMULATION OF THE PROBLEM

It is assumed that there are two collinear interface cracks of length $1-b$ between two dissimilar functionally graded piezoelectric/piezomagnetic material half-planes as shown in Fig. 1. $2b$ is the distance between two collinear cracks (The solution of two collinear cracks of length $d-b$ in functionally graded piezoelectric/piezomagnetic materials can be easily obtained by a simple change in the numerical values of the present paper for crack length $1-b/d$, $d>b>0$.) It is also assumed that the propagation direction of the harmonic elastic anti-plane shear stress wave is vertical to the crack in functionally graded piezoelectric/piezomagnetic materials. Let ω be the circular frequency of the incident wave. $w_0^{(i)}(x,y,t)$, $\phi_0^{(i)}(x,y,t)$, and $\psi_0^{(i)}(x,y,t)(i=1,2)$ are the mechanical displacement, the electric potential, and the magnetic potential, respectively. $\tau_{zk0}^{(i)}(x,y,t)$, $D_{k0}^{(i)}(x,y,t)$, and $B_{k0}^{(i)}(x,y,t)$ $(k=x,y,i=1,2)$ are the anti-plane shear stress field, in-plane electric displacement field, and in-plane magnetic flux, respectively. Also note that all quantities with superscript i $(i=1,2)$ refer to the upper half-plane 1 and the lower half-plane 2 as shown in Fig. 1, respectively. Because the incident waves are harmonic anti-plane shear stress waves, all field quantities $w_0^{(i)}(x,y,t)$, $\phi_0^{(i)}(x,y,t)$, $\psi_0^{(i)}(x,y,t)$, $\tau_{zk0}^{(i)}(x,y,t)$, $D_{k0}^{(i)}(x,y,t)$, and $B_{k0}^{(i)}(x,y,t)$ can be assumed to be of the forms as follows

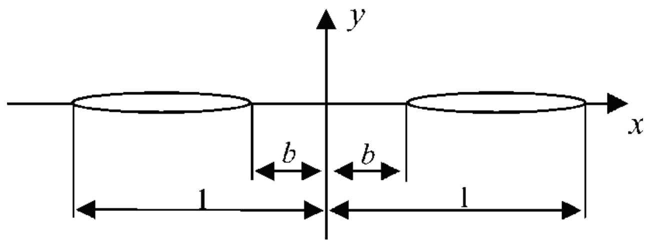

Fig. 1 Geometry and coordinate system for two collinear cracks

$$\begin{aligned}&[w_0^{(i)}(x,y,t),\ \phi_0^{(i)}(x,y,t),\ \psi_0^{(i)}(x,y,t),\\&\quad\tau_{zk0}^{(i)}(x,y,t),\ D_{k0}^{(i)}(x,y,t),\ B_{k0}^{(i)}(x,y,t)]\\&=[w^{(i)}(x,y),\ \phi^{(i)}(x,y),\ \psi^{(i)}(x,y),\\&\quad\tau_{zk}^{(i)}(x,y),\ D_k^{(i)}(x,y),\ B_k^{(i)}(x,y)]\mathrm{e}^{-i\omega t}\end{aligned}\tag{1}$$

In what follows, the time dependence of $\mathrm{e}^{-i\omega t}$ will be suppressed but understood. The functionally graded piezoelectric/piezomagnetic materials boundary-value problem for the harmonic anti-plane shear waves is considerably simplified if only the out-of-plane mechanical displacements, the in-plane electric fields, and the in-plane magnetic fields are considered. As discussed in references [**25**, **26**], as no opening displacement exists for the present anti-plane problem, the crack surfaces can be assumed to be in perfect contact. Accordingly, permeable condition will be enforced in the present study, i.e. the electric potential, the magnetic potential, the normal electric displacement, and the magnetic flux are assumed to be continuous across the crack surfaces. Here, the standard superposition technique was used in the present paper. Therefore, the boundary conditions of the present problem are

(In this paper, we just consider the perturbation fields.)

$$\begin{cases} \tau_{yz}^{(1)}(x,0^+) = \tau_{yz}^{(2)}(x,0^-) = -\tau_0, \quad b \leqslant |x| \leqslant 1 \\ \tau_{yz}^{(1)}(x,0^+) = \tau_{yz}^{(2)}(x,0^-), w^{(1)}(x,0^+) \\ \qquad = w^{(2)}(x,0^-), \quad |x| > 1, \quad |x| < b \end{cases} \tag{2}$$

$$\begin{cases} \phi^{(1)}(x,0^+) = \phi^{(2)}(x,0^-), D_y^{(1)}(x,0^+) = D_y^{(2)}(x,\ 0^-) \\ \psi^{(1)}(x,0^+) = \psi^{(2)}(x,0^-), B_y^{(1)}(x,0^+) = B_y^{(2)}(x,\ 0^-), \\ \qquad |x| \leqslant \infty \end{cases} \tag{3}$$

$$\begin{cases} w^{(1)}(x,y) = w^{(2)}(x,y) = 0 \\ \phi^{(1)}(x,y) = \phi^{(2)}(x,y) = 0 \quad \text{for } (x^2+y^2)^{1/2} \to \infty \\ \psi^{(1)}(x,y) = \psi^{(2)}(x,y) = 0 \end{cases} \tag{4}$$

where τ_0 is a magnitude of the incident wave.

Crack problems in the non-homogeneous piezoelectric/piezomagnetic materials do not appear to be analytically tractable for arbitrary variations of material properties. Usually, one tries to generate the forms of non-homogeneities for which the problem becomes tractable. Similar to the treatment of the crack problem for isotropic non-homogeneous materials in references [**15**–**22**, **27**–**29**], the material properties are described by

$$\begin{cases} c_{44}^{(1)} = c_{440}^{(1)} e^{\beta^{(1)} y}, \quad e_{15}^{(1)} = e_{150}^{(1)} e^{\beta^{(1)} y}, \\ \quad \varepsilon_{11}^{(1)} = \varepsilon_{110}^{(1)} e^{\beta^{(1)} y} \\ q_{15}^{(1)} = q_{150}^{(1)} e^{\beta^{(1)} y}, \quad d_{11}^{(1)} = d_{110}^{(1)} e^{\beta^{(1)} y}, \\ \quad \mu_{11}^{(1)} = \mu_{110}^{(1)} e^{\beta^{(1)} y}, \quad \rho^{(1)}(y) = \rho_0^{(1)} e^{\beta^{(1)} y} \\ c_{44}^{(2)} = c_{440}^{(2)} e^{\beta^{(2)} y}, \quad e_{15}^{(2)} = e_{150}^{(2)} e^{\beta^{(2)} y}, \\ \quad \varepsilon_{11}^{(2)} = \varepsilon_{110}^{(2)} e^{\beta^{(2)} y} \\ q_{15}^{(2)} = q_{150}^{(2)} e^{\beta^{(2)} y}, \quad d_{11}^{(2)} = d_{110}^{(2)} e^{\beta^{(2)} y}, \\ \quad \mu_{11}^{(2)} = \mu_{110}^{(2)} e^{\beta^{(2)} y}, \quad \rho^{(2)}(y) = \rho_0^{(2)} e^{\beta^{(2)} y} \end{cases} \tag{5}$$

where $c_{440}^{(i)}$, $e_{150}^{(i)}$, $\varepsilon_{110}^{(i)}$, $q_{150}^{(i)}$, $d_{150}^{(i)}$, $\mu_{110}^{(i)}$, $\rho_0^{(i)}$, and $\beta^{(i)}$ are the shear modulus, the piezoelectric coefficient, the dielectric parameter, the piezomagnetic coefficient, the magnetoelectric coefficient, the magnetic permeability, the mass density, and the functionally graded parameter of two dissimilar functionally graded piezoelectric/piezomagnetic material half-planes, respectively.

The constitutive equations for the mode III crack can be expressed as

$$\tau_{zk}^{(i)} = c_{44}^{(i)} w_{,k}^{(i)} + e_{15}^{(i)} \phi_{,k}^{(i)} + q_{15}^{(i)} \psi_{,k}^{(i)} \quad (k = x, y, i = 1, 2) \tag{6}$$

$$D_k^{(i)} = e_{15}^{(i)} w_{,k}^{(i)} - \varepsilon_{11}^{(i)} \phi_{,k}^{(i)} - d_{11}^{(i)} \psi_{,k}^{(i)} \quad (k = x, y, i = 1, 2) \tag{7}$$

$$B_k^{(i)} = q_{15}^{(i)} w_{,k}^{(i)} - d_{11}^{(i)} \phi_{,k}^{(i)} - \mu_{11}^{(i)} \psi_{,k}^{(i)} \quad (k = x, y, i = 1, 2) \tag{8}$$

The anti-plane governing equations are [**1**, **2**]

$$c_{440}^{(i)}\left(\nabla^2 w^{(i)} + \beta^{(i)} \frac{\partial w^{(i)}}{\partial y}\right) + e_{150}^{(i)}\left(\nabla^2 \phi^{(i)} + \beta^{(i)} \frac{\partial \phi^{(i)}}{\partial y}\right) + q_{150}^{(i)}\left(\nabla^2 \psi^{(i)} + \beta^{(i)} \frac{\partial \psi^{(i)}}{\partial y}\right) = -\rho_0^{(i)} \omega^2 w^{(i)} \tag{9}$$

$$e_{150}^{(i)}\left(\nabla^2 w^{(i)} + \beta^{(i)} \frac{\partial w^{(i)}}{\partial y}\right) - \varepsilon_{110}^{(i)}\left(\nabla^2 \phi^{(i)} + \beta^{(i)} \frac{\partial \phi^{(i)}}{\partial y}\right) - d_{110}^{(i)}\left(\nabla^2 \psi^{(i)} + \beta^{(i)} \frac{\partial \psi^{(i)}}{\partial y}\right) = 0 \tag{10}$$

$$q_{150}^{(i)}\left(\nabla^2 w^{(i)} + \beta^{(i)} \frac{\partial w^{(i)}}{\partial y}\right) - d_{110}^{(i)}\left(\nabla^2 \phi^{(i)} + \beta^{(i)} \frac{\partial \phi^{(i)}}{\partial y}\right) - \mu_{110}^{(i)}\left(\nabla^2 \psi^{(i)} + \beta^{(i)} \frac{\partial \psi^{(i)}}{\partial y}\right) = 0 \tag{11}$$

where

$$-\rho_0^{(i)} \omega^2 w^{(i)}(x,y) e^{-i\omega t} = \rho_0^{(i)} \frac{\partial^2 w_0^{(i)}(x,y,t)}{\partial t^2} = \rho_0^{(i)} \frac{\partial^2 (w^{(i)}(x,y) e^{-i\omega t})}{\partial t^2}$$

and $\nabla^2 = \partial^2/\partial x^2 + \partial^2/\partial y^2$ is the two-dimensional Laplace operator.

3 SOLUTIONS

Because of the assumed symmetry in geometry and loading, it is sufficient to consider the problem for $0 \leqslant x < \infty$, $-\infty \leqslant y < \infty$ only. The system of the earlier governing equations (9) to (11) is solved using the Fourier integral transform technique to obtain the general expressions for the displacement components, the electric potentials, and the magnetic potentials as

$$\begin{cases} w^{(1)}(x,y) = \dfrac{2}{\pi} \displaystyle\int_0^\infty A_1(s) e^{-\gamma_1^{(1)} y} \cos(sx) ds \\ \phi^{(1)}(x,y) = a_0^{(1)} w^{(1)}(x,y) + \dfrac{2}{\pi} \displaystyle\int_0^\infty B_1(s) e^{-\gamma_2^{(1)} y} \cos(sx) ds \quad (y \geqslant 0) \\ \psi^{(1)}(x,y) = a_1^{(1)} w^{(1)}(x,y) + \dfrac{2}{\pi} \displaystyle\int_0^\infty C_1(s) e^{-\gamma_2^{(1)} y} \cos(sx) ds \end{cases} \tag{12}$$

$$\begin{cases} w^{(2)}(x,y) = \dfrac{2}{\pi} \displaystyle\int_0^\infty A_2(s) e^{-\gamma_1^{(2)} y} \cos(sx) ds \\ \phi^{(2)}(x,y) = a_0^{(2)} w^{(2)}(x,y) + \dfrac{2}{\pi} \displaystyle\int_0^\infty B_2(s) e^{-\gamma_2^{(2)} y} \cos(sx) ds \quad (y \leqslant 0) \\ \psi^{(2)}(x,y) = a_1^{(2)} w^{(2)}(x,y) + \dfrac{2}{\pi} \displaystyle\int_0^\infty C_2(s) e^{-\gamma_2^{(2)} y} \cos(sx) ds \end{cases} \tag{13}$$

where $A_1(s)$, $B_1(s)$, $C_1(s)$, $A_2(s)$, $B_2(s)$, $C_2(s)$ are unknown functions

$$\gamma_1^{(1)} = \frac{\beta^{(1)} + \sqrt{\beta^{(1)2} + 4[s^2 - \omega^2/c_1^2]}}{2}$$

$$\gamma_2^{(1)} = \frac{\beta^{(1)} + \sqrt{\beta^{(1)2} + 4s^2}}{2}, \quad c_1 = \sqrt{\frac{\mu_0^{(1)}}{\rho_0^{(1)}}}$$

$$\mu_0^{(1)} = c_{440}^{(1)} + a_0^{(1)} e_{150}^{(1)} + a_1^{(1)} q_{150}^{(1)}$$

$$a_0^{(1)} = \frac{\mu_{110}^{(1)} e_{150}^{(1)} - d_{110}^{(1)} q_{150}^{(1)}}{\varepsilon_{110}^{(1)} \mu_{110}^{(1)} - d_{100}^{(1)2}}$$

$$a_1^{(1)} = \frac{q_{150}^{(1)} \varepsilon_{110}^{(1)} - d_{11} e_{150}^{(1)}}{\varepsilon_{110}^{(1)} \mu_{110}^{(1)} - d_{100}^{(1)2}}$$

$$\gamma_1^{(2)} = \frac{\beta^{(2)} + \sqrt{\beta^{(2)2} + 4[s^2 - \omega^2/c_2^2]}}{2}$$

$$\gamma_2^{(2)} = \frac{\beta^{(2)} + \sqrt{\beta^{(2)2} + 4s^2}}{2}, \quad c_2 = \sqrt{\frac{\mu_0^{(2)}}{\rho_0^{(2)}}}$$

$$\mu_0^{(2)} = c_{440}^{(2)} + a_0^{(2)} e_{150}^{(2)} + a_1^{(2)} q_{150}^{(2)}$$

$$a_0^{(2)} = \frac{\mu_{110}^{(2)} e_{150}^{(2)} - d_{110}^{(2)} q_{150}^{(2)}}{\varepsilon_{110}^{(2)} \mu_{110}^{(2)} - d_{110}^{(2)2}}$$

$$a_1^{(2)} = \frac{q_{150}^{(2)} \varepsilon_{110}^{(2)} - d_{110}^{(2)} e_{150}^{(2)}}{\varepsilon_{110}^{(2)} \mu_{110}^{(2)} - d_{110}^{(2)2}}$$

Therefore, from equations (6) to (8), it can be obtained

$$\begin{aligned}\tau_{yz}^{(1)}(x, y) = -\frac{2e^{\beta^{(1)}y}}{\pi} \int_0^\infty \{\mu_0^{(1)} \gamma_1^{(1)} A_1(s) e^{-\gamma_1^{(1)} y} \\ + \gamma_2^{(1)} [e_{150}^{(1)} B_1(s) + q_{150}^{(1)} C_1(s)] e^{-\gamma_2^{(1)} y}\} \\ \times \cos(sx) ds\end{aligned} \tag{14}$$

$$\begin{aligned}D_y^{(1)}(x, y) = \frac{2e^{\beta^{(1)}y}}{\pi} \int_0^\infty \gamma_2^{(1)} [\varepsilon_{110}^{(1)} B_1(s) \\ + d_{110}^{(1)} C_1(s)] e^{-\gamma_2^{(1)} y} \cos(sx) ds\end{aligned} \tag{15}$$

$$\begin{aligned}B_y^{(1)}(x, y) = \frac{2e^{\beta^{(1)}y}}{\pi} \int_0^\infty \gamma_2^{(1)} [d_{110}^{(1)} B_1(s) \\ + \mu_{110}^{(1)} C_1(s)] e^{-\gamma_2^{(1)} y} \cos(sx) ds\end{aligned} \tag{16}$$

$$\begin{aligned}\tau_{yz}^{(2)}(x, y) = \frac{2e^{\beta^{(2)}y}}{\pi} \int_0^\infty \{\mu_0^{(2)} \gamma_1^{(2)} A_2(s) e^{\gamma_1^{(2)} y} \\ + \gamma_2^{(2)} [e_{150}^{(2)} B_2(s) \\ + q_{150}^{(2)} C_2(s)] e^{\gamma_2^{(2)} y}\} \cos(sx) ds\end{aligned} \tag{17}$$

$$\begin{aligned}D_y^{(2)}(x, y) = -\frac{2e^{\beta^{(2)}y}}{\pi} \int_0^\infty \gamma_2^{(2)} [\varepsilon_{110}^{(2)} B_2(s) \\ + d_{110}^{(2)} C_2(s)] e^{\gamma_2^{(2)} y} \cos(sx) ds\end{aligned} \tag{18}$$

$$\begin{aligned}B_y^{(2)}(x, y) = -\frac{2e^{\beta^{(2)}y}}{\pi} \int_0^\infty \gamma_2^{(2)} [d_{110}^{(2)} B_2(s) \\ + \mu_{110}^{(2)} C_2(s)] e^{\gamma_2^{(2)} y} \cos(sx) ds\end{aligned} \tag{19}$$

To solve the problem, the jump of the displacements across the crack surfaces is defined as follows

$$f(x) = w^{(1)}(x, 0^+) - w^{(2)}(x, 0^-) \tag{20}$$

Substituting equations (12) and (13) into equation (20), and applying the Fourier transform and the boundary conditions (3), it can be obtained

$$\bar{f}(s) = A_1(s) - A_2(s) \tag{21}$$

$$a_0^{(1)} A_1(s) - a_0^{(2)} A_2(s) + B_1(s) - B_2(s) = 0 \tag{22}$$

$$a_1^{(1)} A_1(s) - a_1^{(2)} A_2(s) + C_1(s) - C_2(s) = 0 \tag{23}$$

A superposed bar indicates the Fourier transform throughout the paper. Substituting equations (14) to (19) into the boundary conditions (2) to (4), it can be obtained

$$\begin{aligned}\mu_0^{(1)} \gamma_1^{(1)} A_1(s) + \gamma_2^{(1)} [e_{150}^{(1)} B_1(s) + q_{150}^{(1)} C_1(s)] \\ + \mu_0^{(2)} \gamma_1^{(2)} A_2(s) + \gamma_2^{(2)} [e_{150}^{(2)} B_2(s) + q_{150}^{(2)} C_2(s)] = 0\end{aligned} \tag{24}$$

$$\begin{aligned}\gamma_2^{(1)} [\varepsilon_{110}^{(1)} B_1(s) + d_{110}^{(1)} C_1(s)] \\ + \gamma_2^{(2)} [\varepsilon_{110}^{(2)} B_2(s) + d_{110}^{(2)} C_2(s)] = 0\end{aligned} \tag{25}$$

$$\begin{aligned}\gamma_2^{(1)} [d_{110}^{(1)} B_1(s) + \mu_{110}^{(1)} C_1(s)] \\ + \gamma_2^{(2)} [d_{110}^{(2)} B_2(s) + \mu_{110}^{(2)} C_2(s)] = 0\end{aligned} \tag{26}$$

By solving six equations (21) to (26) with six unknown functions and substituting the solutions into equations (14) to (16) and applying the boundary conditions (2) and (3), it can be obtained

$$\frac{2}{\pi} \int_0^\infty \bar{f}(s) \cos(sx) ds = 0, \quad x > 1, \quad 0 < x < b \tag{27}$$

$$\frac{2}{\pi} \int_0^\infty g_1(s) \bar{f}(s) \cos(sx) ds = -\tau_0, \quad b \leqslant x \leqslant 1 \tag{28}$$

where $g_1(s)$ is a known function (Appendix 2). $\lim_{s\to\infty} g_1(s)/s = \beta_1$. β_1 is a constant which depends on the properties of the materials (Appendix 2). However, β_1 is independent of the functionally graded parameters $\beta^{(1)}$ and $\beta^{(2)}$. When the properties of the upper and the lower half-planes are continuous along the crack line, $\beta_1 = -c_{440}^{(1)}/2$. To determine the unknown function $\bar{f}(s)$, a pair of triple integral equations (27) and (28) must be solved.

4 SOLUTION OF THE TRIPLE INTEGRAL EQUATIONS

The Schmidt method [**23**] is used to solve the triple integral equations (27) and (28). The jump of the displacements across the crack surfaces is represented by the following series

$$f(x) = \sum_{n=0}^{\infty} b_n P_n^{(1/2,1/2)}\left(\frac{x-(1+b)/2}{(1-b)/2}\right) \times \left(1 - \frac{(x-(1+b)/2)^2}{((1-b)/2)^2}\right)^{1/2}, \quad \text{for } b \leqslant x \leqslant 1 \tag{29}$$

$$f(x) = w^{(1)}(x,0) - w^{(2)}(x,0) = 0, \quad \text{for } x > 1, \quad 0 < x < b \tag{30}$$

where b_n are unknown coefficients to be determined and $P_n^{(1/2,1/2)}(x)$ is a Jacobi polynomial [**30**]. The Fourier transform of equations (29) and (30) is [**31**]

$$\bar{f}(s) = \sum_{n=0}^{\infty} b_n F_n G_n(s) \frac{1}{s} J_{n+1}\left(s\frac{1-b}{2}\right) \tag{31}$$

where

$$F_n = 2\sqrt{\pi}\frac{\Gamma(n+1+(1/2))}{n!},$$

$$G_n(s) = \begin{cases} (-1)^{n/2}\cos\left(s\dfrac{1+b}{2}\right), & n = 0, 2, 4, 6, \ldots \\ (-1)^{(n+1)/2}\sin\left(s\dfrac{1+b}{2}\right), & n = 1, 3, 5, 7, \end{cases}$$

$\Gamma(x)$ and $J_n(x)$ are the Gamma and Bessel functions, respectively.

Substituting equation (31) into equations (27) and (28), equation (27) has been automatically satisfied. After integration with respect to x in $[b, x]$, equation (28) reduces to

$$\frac{2}{\pi}\sum_{n=0}^{\infty} b_n F_n \int_0^{\infty} \frac{1}{s^2} g_1(s) G_n(s) J_{n+1}\left(s\frac{1-b}{2}\right) \times [\sin(sx) - \sin(sb)]\mathrm{d}s = -\tau_0(x-b), \quad \text{for } b \leqslant x \leqslant 1 \tag{32}$$

The semi-infinite integral in equation (32) can be numerically evaluated easily as shown in Appendix 3. Thus, equation (32) can now be solved for the coefficients b_n by the Schmidt method [**23**], as shown in Appendix 4.

5 INTENSITY FACTORS

The coefficients b_n are known, so that the entire perturbation stress field, the perturbation electric displacement field, and the magnetic flux can be obtained. However, in fracture mechanics, it is of importance to determine the perturbation stress $\tau_{yz}^{(1)}$, the perturbation electric displacement $D_y^{(1)}$, and the magnetic flux $B_y^{(1)}$ in the vicinity of the crack tips. In the case of the present study, $\tau_{yz}^{(1)}$, $D_y^{(1)}$, and $B_y^{(1)}$ along the crack line can be expressed, respectively, as

$$\begin{aligned} \tau_{yz}^{(1)}(x,0) &= \frac{2}{\pi}\sum_{n=0}^{\infty} b_n F_n \int_0^{\infty} \frac{1}{s} g_1(s) G_n(s) \times J_{n+1}\left(s\frac{1-b}{2}\right)\cos(xs)\mathrm{d}s \\ &= \frac{2\beta_1}{\pi}\sum_{n=0}^{\infty} b_n F_n \times \int_0^{\infty} G_n(s) J_{n+1}\left(s\frac{1-b}{2}\right)\cos(xs)\mathrm{d}s \\ &\quad + \frac{2}{\pi}\sum_{n=0}^{\infty} b_n F_n \int_0^{\infty}\left[\frac{1}{s}g_1(s) - \beta_1\right] \times G_n(s) J_{n+1}\left(s\frac{1-b}{2}\right)\cos(xs)\mathrm{d}s \end{aligned} \tag{33}$$

$$\begin{aligned} D_y^{(1)}(x,0) &= \frac{2}{\pi}\sum_{n=0}^{\infty} b_n F_n \times \int_0^{\infty} \frac{1}{s} g_2(s) G_n(s) J_{n+1}\left(s\frac{1-b}{2}\right)\cos(xs)\mathrm{d}s \\ &= \frac{2\beta_2}{\pi}\sum_{n=0}^{\infty} b_n F_n \times \int_0^{\infty} G_n(s) J_{n+1}\left(s\frac{1-b}{2}\right)\cos(xs)\mathrm{d}s \\ &\quad + \frac{2}{\pi}\sum_{n=0}^{\infty} b_n F_n \int_0^{\infty}\left[\frac{1}{s}g_2(s) - \beta_2\right] G_n(s) \times J_{n+1}\left(s\frac{1-b}{2}\right)\cos(xs)\mathrm{d}s \end{aligned} \tag{34}$$

$$\begin{aligned} B_y^{(1)}(x,0) &= \frac{2}{\pi}\sum_{n=0}^{\infty} b_n F_n \times \int_0^{\infty} \frac{1}{s} g_3(s) G_n(s) J_{n+1}\left(s\frac{1-b}{2}\right)\cos(xs)\mathrm{d}s \\ &= \frac{2\beta_3}{\pi}\sum_{n=0}^{\infty} b_n F_n \times \int_0^{\infty} G_n(s) J_{n+1}\left(s\frac{1-b}{2}\right)\cos(xs)\mathrm{d}s \\ &\quad + \frac{2}{\pi}\sum_{n=0}^{\infty} b_n F_n \int_0^{\infty}\left[\frac{1}{s}g_3(s) - \beta_3\right] \times G_n(s) J_{n+1}\left(s\frac{1-b}{2}\right)\cos(xs)\mathrm{d}s \end{aligned} \tag{35}$$

where $g_2(s)$ and $g_3(s)$ are known functions (Appendix 2). $\lim_{s\to\infty} g_2(s)/s = \beta_2$ and $\lim_{s\to\infty} g_3(s)/s = \beta_3$, where β_2 and β_3 are two constants which depend on the properties of the materials (Appendix 2). When the properties of the upper and the lower half-planes are continuous along the crack line, $\beta_2 = -e_{150}^{(1)}/2$ and $\beta_3 = -q_{150}^{(1)}/2$.

From the relationships [**30**] as shown in Appendix 5, the singular parts of the stress field, the electric displacement field, and the magnetic flux near the crack tips in equations (33) to (35) can be expressed, respectively, as follows ($x > 1$ or $x < b$)

$$\tau = \frac{\beta_1}{\pi}\sum_{n=0}^{\infty} b_n F_n H_n(b, x) \tag{36}$$

$$D = \frac{\beta_2}{\pi}\sum_{n=0}^{\infty} b_n F_n H_n(b, x) \tag{37}$$

$$B = \frac{\beta_3}{\pi}\sum_{n=0}^{\infty} b_n F_n H_n(b, x) \tag{38}$$

where

$$H_n(b, x) = \begin{cases} (-1)^{n+1} R(b, x, n), & 0 < x < b \\ -R(b, x, n), & x > 1 \end{cases}$$

$$R(b, x, n) = \frac{2(1-b)^{n+1}}{\sqrt{|1+b-2x|^2-(1-b)^2}\left[|1+b-2x| + \sqrt{|1+b-2x|^2-(1-b)^2}\right]^{n+1}}$$

At the left tip of the right crack, the stress intensity factor K_{L} can be expressed as

$$K_{\mathrm{L}} = \lim_{x\to b^-}\sqrt{2(b-x)}\,\tau = -\frac{\beta_1}{\pi}\sqrt{\frac{2}{(1-b)}}\sum_{n=0}^{\infty}(-1)^n b_n F_n \tag{39}$$

At the right tip of the right crack, the stress intensity factor K_{R} can be expressed as

$$K_{\mathrm{R}} = \lim_{x\to 1^+}\sqrt{2(x-1)}\,\tau = -\frac{\beta_1}{\pi}\sqrt{\frac{2}{(1-b)}}\sum_{n=0}^{\infty} b_n F_n \tag{40}$$

At the left tip of the right crack, the electric displacement intensity factor $K_{\mathrm{L}}^{\mathrm{D}}$ can be expressed as

$$K_{\mathrm{L}}^{\mathrm{D}} = \lim_{x\to b^-}\sqrt{2(b-x)}\,D = -\frac{\beta_2}{\pi}\sqrt{\frac{2}{(1-b)}}\sum_{n=0}^{\infty}(-1)^n b_n F_n = \frac{\beta_2}{\beta_1}K_{\mathrm{L}} \tag{41}$$

At the right tip of the right crack, the electric displacement intensity factor $K_{\mathrm{R}}^{\mathrm{D}}$ can be expressed as

$$K_{\mathrm{R}}^{\mathrm{D}} = \lim_{x\to 1^+}\sqrt{2(x-1)}\,D = -\frac{\beta_2}{\pi}\sqrt{\frac{2}{(1-b)}}\sum_{n=0}^{\infty} b_n F_n = \frac{\beta_2}{\beta_1}K_{\mathrm{R}} \tag{42}$$

At the left tip of the right crack, the magnetic flux intensity factor $K_{\mathrm{L}}^{\mathrm{B}}$ can be expressed as

$$K_{\mathrm{L}}^{\mathrm{B}} = \lim_{x\to b^-}\sqrt{2(b-x)}\,B = -\frac{\beta_3}{\pi}\sqrt{\frac{2}{(1-b)}}\sum_{n=0}^{\infty}(-1)^n b_n F_n = \frac{\beta_3}{\beta_1}K_{\mathrm{L}} \tag{43}$$

At the right tip of the right crack, the magnetic flux intensity factor $K_{\mathrm{R}}^{\mathrm{B}}$ can be expressed as

$$K_{\mathrm{R}}^{\mathrm{B}} = \lim_{x\to 1^+}\sqrt{2(x-1)}\,D = -\frac{\beta_3}{\pi}\sqrt{\frac{2}{(1-b)}}\sum_{n=0}^{\infty} b_n F_n = \frac{\beta_3}{\beta_1}K_{\mathrm{R}} \tag{44}$$

6 NUMERICAL CALCULATIONS AND DISCUSSION

From the literatures [**21–23**], it can be seen that the Schmidt method performs satisfactorily if the first 10 terms of the infinite series (32) are retained. At $b \leqslant x \leqslant 1, y = 0$, it can be obtained that $\tau_{yz}^{(1)}/\tau_0$ is very close to negative unity. Hence, the solution of the present paper can also be proved to satisfy the boundary conditions (2). In all computations, according to references [**1, 2, 9**], the constants of materials-I are assumed to be $c_{440}^{(1)} = 44.0$ (GPa), $e_{150}^{(1)} = 5.8$ (C/m^2), $\varepsilon_{110}^{(1)} = 5.64 \times 10^{-9}$ (C^2/N m^2), $q_{150}^{(1)} = 275.0$ (N/A m), $d_{110}^{(1)} = 0.005 \times 10^{-9}$ (N s/V C), $\mu_{110}^{(1)} = -297.0 \times 10^{-6}$ (N s^2/C^2), $\rho_0^{(1)} = 1500\,\mathrm{kg/m^3}$ and the constants of materials-II are assumed to be $c_{440}^{(2)} = 34.0$ (GPa), $e_{150}^{(2)} = 4.8$ (C/m^2), $\varepsilon_{110}^{(2)} = 4.64 \times 10^{-9}$ (C^2/N m^2), $q_{150}^{(2)} = 195.0$ (N/A m), $d_{110}^{(2)} = 0.004 \times 10^{-9}$ (N s/V C), $\mu_{110}^{(2)} = -201.0 \times 10^{-6}$ (N s^2/C^2), $\rho_0^{(2)} = 1000\,\mathrm{kg/m^3}$. The normalized non-homogeneity constants $\beta^{(i)} (i = 1, 2)$ are varied between -2 and 2, which covers most of the practical cases. The results of the present paper are shown in Figs 2 to 10. From the results, the following observations are very significant.

1. From the results, it can be shown that the singular stress, electric displacement, and the magnetic flux in the functionally graded piezoelectric/piezomagnetic materials carry the same forms as those

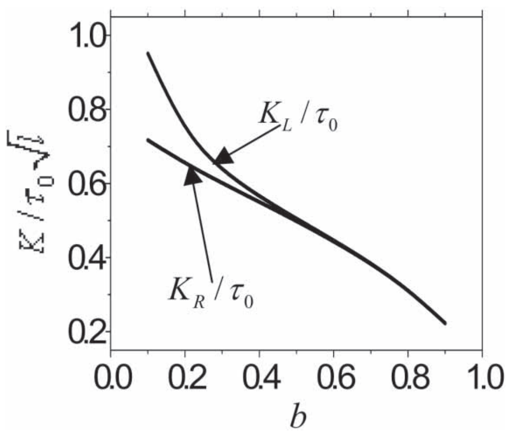

Fig. 2 The stress intensity factor versus b for $\omega/c_1 = 0.4$, $\beta^{(1)} = 0.2$, and $\beta^{(2)} = 0.4$ (material-I/material-II)

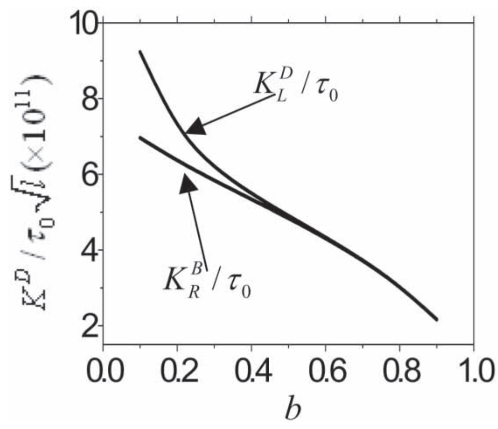

Fig. 3 The electric displacement intensity factor versus b for $\omega/c_1 = 0.4, \beta^{(1)} = 0.2$, and $\beta^{(2)} = 0.4$ (material-I/material-II)

in the homogeneous piezoelectric/piezomagnetic materials or in the homogeneous piezoelectric materials, but the magnitudes of the intensity factors depend significantly upon the gradient of the functionally graded piezoelectric/piezomagnetic materials properties as discussed in references [**19–22**].

2. The magneto-electro-elastic coupling effects can be obtained as shown in equations (39)–(44). For the electric displacement and the magnetic flux intensity factors, they have the same changing tendency as the stress intensity factors as shown in Figs 2 to 4. However, the amplitude values of the electric displacement field, the magnetic flux field, and the stress field are different. The amplitude values of the electric displacement and the magnetic flux fields are very small as shown in Figs 3 and 4. The results of the electric displacement and the magnetic flux intensity factors can be directly obtained from the results of the stress intensity factors through equations (39) to (44). This means that an applied mechanical load alone can produce the electric displacement and magnetic flux singularities. The results of the electric displacement and the magnetic flux intensity factors of the other cases have been omitted in the present paper.
3. The interaction of the two collinear cracks decreases when the distance between the two collinear cracks increases as shown in Figs 2 to 4. The intensity factors at the inner crack tips are bigger than those at the outer crack tips. However, the intensity factors at the inner and outer crack tips are almost overlapped for $b \geqslant 0.5$ as shown in Figs 2 to 4. When the material properties of the upper half-plane are equal to the ones of the lower half-plane along the crack line, it can obtain the same conclusion as shown in Figs 7 and 10. It can also be obtained that this conclusion is the same as the dynamic anti-plane shear fracture problem in the isotropic homogeneous materials.
4. The dynamic stress intensity factors tend to increase with the frequency of incident waves, reaching a peak and then to decrease in magnitude as shown in Figs 5 to 7. The intensity factors at the inner crack tips are bigger than those at the outer crack tips for $\omega/c_1 < 2.3$. However, the intensity factors at the inner crack tips are smaller than those at the outer crack tips for $\omega/c_1 > 2.3$ as shown in Figs 5 to 7. These phenomena may be caused by the coupling effects of the mechanical field, the electric field, and the magnetic flux field. From the results, it can be concluded that the stress, the electric

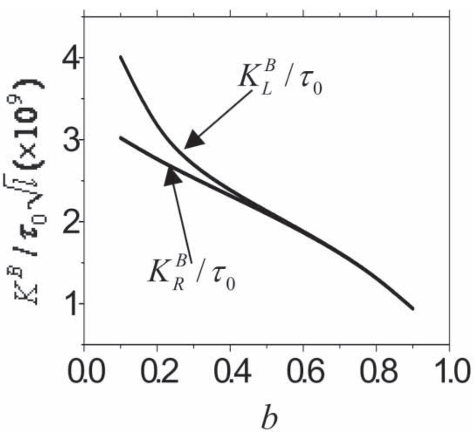

Fig. 4 The magnetic flux intensity factor versus b for $\omega/c_1 = 0.4, \beta^{(1)} = 0.2$, and $\beta^{(2)} = 0.4$ (material-I/material-II)

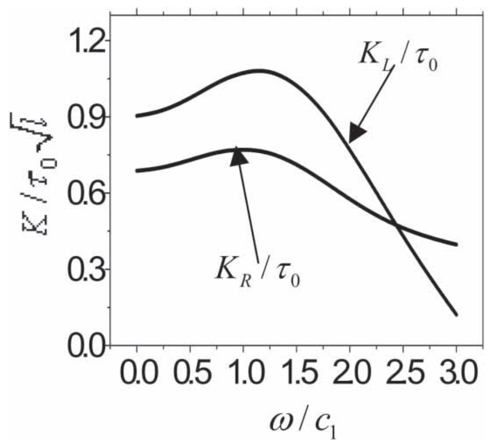

Fig. 5 The stress intensity factor versus ω/c_1 for $b = 0.1$, $\beta^{(1)} = 0.2$, and $\beta^{(2)} = 0.4$ (material-I/material-II)

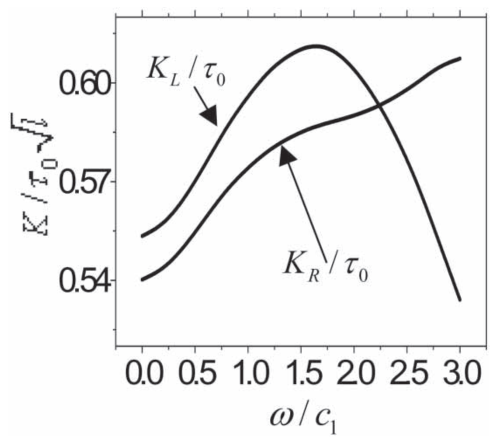

Fig. 6 The stress intensity factor versus ω/c_1 for $b = 0.4$, $\beta^{(1)} = 0.2$, and $\beta^{(2)} = 0.4$ (material-I/material-II)

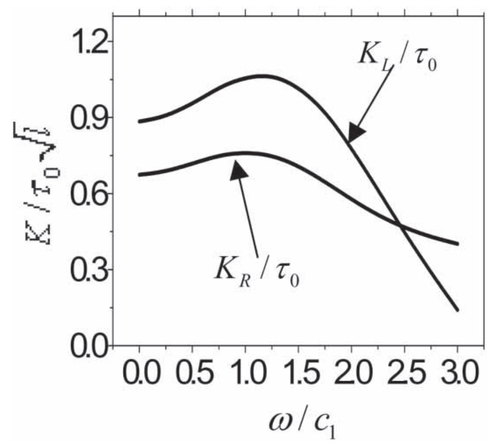

Fig. 7 The stress intensity factor versus ω/c_1 for $b = 0.1$, $\beta^{(1)} = 0.4$, and $\beta^{(2)} = 0.4$ (material-I/material-I)

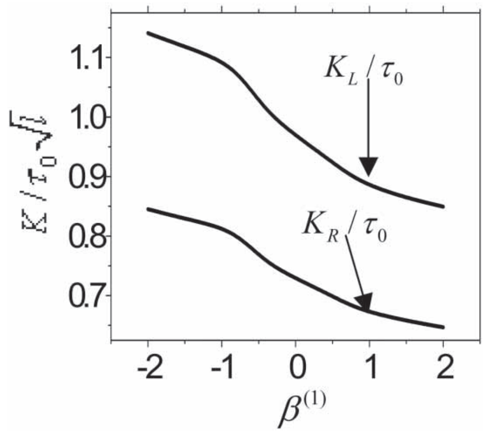

Fig. 8 The stress intensity factor versus $\beta^{(1)}$ for $\omega/c_1 = 0.4$, $b = 0.1$, and $\beta^{(2)} = 0.4$ (material-I/material-II)

displacement, and the magnetic fields near the crack tips can be deduced by adjusting the frequency of incident waves in engineering practices.

5. The stress intensity factors tend to decrease with increase in the functionally graded parameters $\beta^{(i)} (i = 1, 2)$ as shown in Figs 8 to 10. When the material properties of the upper half-plane and the lower half-plane along the crack line are continuous, it can obtain the same conclusion as shown in Fig. 10. This means that, by adjusting the functionally graded parameters, the dynamic stress fields near the crack tips can be reduced.
6. The solution of the present paper can revert to one of the problems which the material properties of

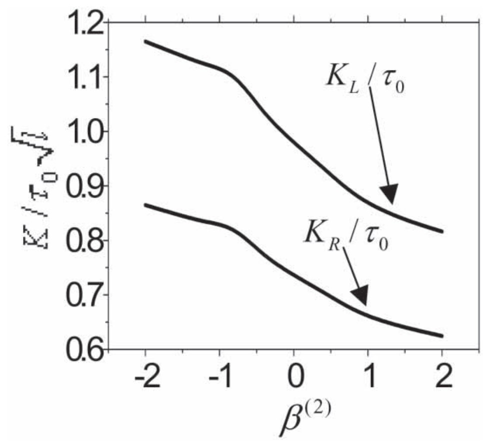

Fig. 9 The stress intensity factor versus $\beta^{(2)}$ for $\omega/c_1 = 0.4$, $b = 0.1$, and $\beta^{(1)} = 0.4$ (material-I/material-II)

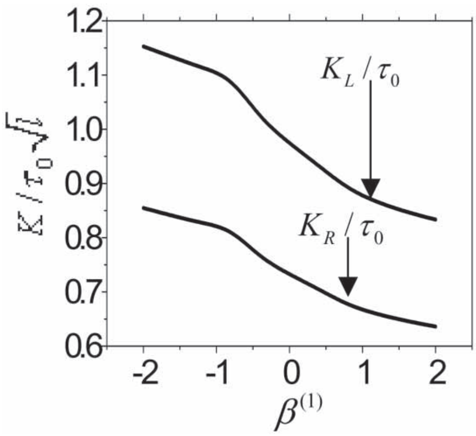

Fig. 10 The stress intensity factor versus $\beta^{(1)}$ for $\omega/c_1 = 0.4$, $b = 0.1$, and $\beta^{(2)} = 0.4$ (material-I/material-I)

the upper half-plane and the lower half-plane along the crack line are continuous as shown in Figs 7 and 10.

ACKNOWLEDGEMENTS

The authors are grateful for the financial support by the National Natural Science Foundation of China (10 572 043, 10 572 155, 50 232 030, 10 172 030), the Natural Science Foundation with Excellent Young Investigators of Hei Long Jiang Province (JC04-08), and the Natural Science Foundation of Hei Long Jiang Province (A0301).

REFERENCES

1 **Sih, G. C.** and **Song, Z. F.** Magnetic and electric poling effects associated with crack growth in $BaTiO_3$–$CoFe_2O_4$ composite. *Theor. Appl. Fract. Mech.*, 2003, **39**, 209–227.

2 **Song, Z. F.** and **Sih, G. C.** Crack initiation behavior in magnetoelectroelastic composite under in-plane deformation. *Theor. Appl. Fract. Mech.*, 2003, **39**, 189–207.

3 **Wang, B. L.** and **Mai, Y. W.** Crack tip field in piezoelectric/piezomagnetic media. *Eur. J. Mech. A/Solid*, 2003, **22**(4), 591–602.

4 **Wang, B. L.** and **Mai, Y. W.** Fracture of piezoelectromagnetic materials. *Mech. Res. Commun.*, 2004, **31**(1), 65–73.

5 **Gao, C. F., Tong, P.,** and **Zhang, T. Y.** Interfacial crack problems in magneto–electroelastic solids. *Int. J. Eng. Sci.*, 2003, **41**(18), 2105–2121.

6 **Gao, C. F., Kessler, H.,** and **Balke, H.** Fracture analysis of electromagnetic thermoelastic solids. *Eur. J. Mech. A/Solid*, 2003, **22**(3), 433–442.

7 **Gao, C. F., Kessler, H.,** and **Balke, H.** Crack problems in magnetoelectroelastic solids. Part I: exact solution of a crack. *Int. J. Eng. Sci.*, 2003, **41**(9), 969–981.

8 **Gao, C. F., Kessler, H.,** and **Balke, H.** Crack problems in magnetoelectroelastic solids. Part II: general solution of collinear cracks. *Int. J. Eng. Sci.*, 2003, **41**(9), 983–994.

9 **Spyropoulos, C. P., Sih, G. C.,** and **Song, Z. F.** Magnetoelectroelastic composite with poling parallel to plane of line crack under out-of-plane deformation. *Theor. Appl. Fract. Mech.*, 2003, **39**(3), 281–289.

10 **Liu, J. X., Liu, X. L.,** and **Zhao, Y. B.** Green's functions for anisotropic magnetoelectroelastic solids with an elliptical cavity or a crack. *Int. J. Eng. Sci.*, 2001, **39**(12), 1405–1418.

11 **Zhou, Z. G., Wu, L. Z.,** and **Wang, B.** The dynamic behavior of two collinear interface cracks in magneto–electro–elastic composites. *Eur. J. Mech. A/Solids*, 2005, **24**(2), 253–262.

12 **Zhou, Z. G., Wang, B.,** and **Sun, Y. G.** Two collinear interface cracks in magneto–electro–elastic composites. *Int. J. Eng. Sci.*, 2004, **42**, 1157–1167.

13 **Takagi, K., Li, J. F., Yokoyama, S.,** and **Watanabe, R.** Fabrication and evaluation of PZT/Pt piezoelectric composites and functionally graded actuators. *J. Eur. Ceramic Soc.*, 2003, **10**, 1577–1583.

14 **Jin, D. R.** Functionally graded PZT/ZnO piezoelectric composites. *J. Mater. Sci. Lett.*, 2003, **22**, 971–974.

15 **Chen, J., Liu, Z. X.,** and **Zou, Z. Z.** Electromechanical impact of a crack in a functionally graded piezoelectric medium. *Theor. Appl. Fract. Mech.*, 2003, **39**, 47–60.

16 **Jin, B.** and **Zhong, Z.** A moving mode-III crack in functionally graded piezoelectric material: permeable problem. *Mech. Res. Commun.*, 2002, **29**, 217–224.

17 **Wang, B. L.** A mode-III crack in functionally graded piezoelectric materials. *Mech. Res. Commun.*, 2003, **30**, 151–159.

18 **Kwon, S. M.** Electrical nonlinear anti-plane shear crack in a functionally graded piezoelectric strip. *Int. J. Solid. Struct.*, 2003, **40**, 5649–5667.

19 **Li, C. Y.** and **Weng, G. J.** Antiplane crack problem in functionally graded piezoelectric materials. *J. Appl. Mech.*, 2002, **69**(4), 481–488.

20 **Sun, J. L., Zhou, Z. G.,** and **Wang, B.** Dynamic behavior of a crack in a functionally graded piezoelectric strip bonded to two dissimilar half piezoelectric material planes. *ACTA Mech.*, 2005, **176**(1–2), 45–60.

21 **Zhou, Z. G.** and **Wang, B.** Two parallel symmetry permeable cracks in functionally graded piezoelectric/piezomagnetic materials under anti-plane shear loading. *Int. J. Solid. Struct.*, 2004, **41**, 4407–4422.

22 **Zhou, Z. G., Wu, L. Z.,** and **Wang, B.** The behavior of a crack in functionally graded piezoelectric/piezomagnetic materials under anti-plane shear loading. *Arch. Appl. Mech.*, 2005, **74**(8), 526–535.

23 **Morse, P. M.** and **Feshbach, H.** *Methods of theoretical physics*, vol. 1, 1958 (McGraw-Hill, New York).

24 **Zhou, Z. G., Han, J. C.,** and **Du, S. Y.** Investigation of a crack subjected to anti-plane shear by using the non-local theory. *Int. J. Solid. Struct.*, 1999, **36**(26), 3891–3901.

25 **Soh, A. K., Fang, D. N.,** and **Lee, K. L.** Analysis of a bi-piezoelectric ceramic layer with an interfacial crack subjected to anti-plane shear and in-plane electric loading. *Eur. J. Mech. A/Solid*, 2000, **19**, 961–977.

26 **Srivastava, K. N., Palaiya, K. N.,** and **Karaulia, D. S.** Interaction of shear waves with two coplanar Griffith cracks situated in an infinitely long elastic strip. *Int. J. Fract.*, 1983, **23**, 3–14.
27 **Delale, F.** and **Erdogan, F.** On the mechanical modeling of the interfacial region in bonded half-planes. *ASME J. Appl. Mech.*, 1988, **55**, 317–324.
28 **Fildis, H.** and **Yahsi, O. S.** The axisymmetric crack problem in a non-homogeneous interfacial region between homogeneous half-spaces. *Int. J. Fract.*, 1996, **78**, 139–163.
29 **Ozturk, M.** and **Erdogan, F.** Mode I crack problem in an inhomogeneous orthotropic medium. *Int. J. Eng. Sci.*, 1997, **35**, 869–883.
30 **Gradshteyn, I. S.** and **Ryzhik, I. M.** *Table of integral, series and products*, 1980 (Academic Press, New York).
31 **Erdelyi, A.** (Ed.) *Tables of integral transforms*, vol. 1, 1954 (McGraw-Hill, New York).

APPENDIX 1

Notation

$a_0^{(i)}$	the known constants
$a_1^{(i)}$	the known constants
$A_1(s)$	an unknown function
$A_2(s)$	an unknown function
b	the half-distance between two collinear cracks
b_n	the unknown coefficients
$B_1(s)$	an unknown function
$B_2(s)$	an unknown function
$B_{k0}^{(i)}(x, y, t)$	in-plane magnetic flux
$B_k^{(i)}(x, y)$	the amplitude of $B_{k0}^{(i)}(x, y, t)$
c_i	the shear wave velocities
c_{440}^i	the shear modulus
$C_1(s)$	an unknown function
$C_2(s)$	an unknown function
$d_{150}^{(i)}$	the magnetioelectric coefficients
$D_{k0}^{(i)}(x, y, t)$	in-plane electric displacement fields
$D_k^{(i)}(x, y)$	the amplitude of $D_{k0}^{(i)}(x, y, t)$
$e_{150}^{(i)}$	the piezoelectric coefficients
$f(x)$	the jump of the displacements across the crack surfaces
$g_1(s)$	a known function
$g_2(s)$	a known function
$g_3(s)$	a known function
$G_n(s)$	the known functions
$J_n(x)$	the Bessel functions
K_{L}	the stress intensity factor at the left tip of the right crack
K_{R}	the stress intensity factor at the right tip of the right crack
$K_{\mathrm{L}}^{\mathrm{B}}$	the magnetic flux intensity factor at the left tip of the right crack
$K_{\mathrm{R}}^{\mathrm{B}}$	the magnetic flux intensity factor at the right tip of the right crack
$K_{\mathrm{L}}^{\mathrm{D}}$	the electric displacement intensity factor at the left tip of the right crack
$K_{\mathrm{R}}^{\mathrm{B}}$	the electric displacement intensity factor at the right tip of the right crack
$P_n^{(1/2,\,1/2)}(x)$	the Jacobi polynomials
$q_{150}^{(i)}$	the piezomagnetic coefficients
$w_0^{(i)}(x, y, t)$	the mechanical displacements
$w^{(i)}(x, y)$	the amplitude of $w_0^{(i)}(x, y, t)$
β_1	a known constant
β_2	a known constant
β_3	a known constant
$\beta^{(i)}$	the functionally graded parameters
$\gamma_1^{(i)}$	the known functions
$\gamma_2^{(i)}$	the known functions
$\gamma(x)$	the Gamma function
$\varepsilon_{110}^{(i)}$	the dielectric parameters
$\mu_{110}^{(i)}$	the magnetic permeability
$\mu_0^{(i)}$	the known constants
$\rho_0^{(i)}$	the mass densities
$\tau_{zk0}^{(i)}(x, y, t)$	the anti-plane shear stress fields
$\tau_{zk}^{(i)}(x, y)$	the amplitude of $\tau_{zk0}^{(i)}(x, y, t)$
τ_0	the magnitude of the incident wave
$\phi_0^{(i)}(x, y, t)$	the electric potentials
$\phi^{(i)}(x, y)$	the amplitude of $\phi_0^{(i)}(x, y, t)$
$\psi_0^{(i)}(x, y, t)$	the magnetic potentials
$\psi^{(i)}(x, y)$	the amplitude of $\psi_0^{(i)}(x, y, t)$
ω	the circular frequency of the incident wave
∇^2	the two-dimensional Laplace operator

APPENDIX 2

The functions of $g_1(s)$, $g_2(s)$, and $g_3(s)$ can be obtained by the operation of the following matrixes

$$[\mathbf{X}_1] = \begin{bmatrix} 1 & 0 & 0 \\ a_0^{(1)} & 1 & 0 \\ a_1^{(1)} & 0 & 1 \end{bmatrix}, \quad [\mathbf{X}_2] = \begin{bmatrix} -1 & 0 & 0 \\ -a_0^{(2)} & -1 & 0 \\ -a_1^{(2)} & 0 & -1 \end{bmatrix}$$

$$[\mathbf{X}_3] = \begin{bmatrix} \mu_0^{(1)}\gamma_1^{(1)} & \gamma_2^{(1)} e_{150}^{(1)} & \gamma_2^{(1)} q_{150}^{(1)} \\ 0 & \gamma_2^{(1)} \varepsilon_{110}^{(1)} & \gamma_2^{(1)} d_{110}^{(1)} \\ 0 & \gamma_2^{(1)} d_{110}^{(1)} & \gamma_2^{(1)} \mu_{110}^{(1)} \end{bmatrix}$$

$$[\mathbf{X}_4] = \begin{bmatrix} \mu_0^{(2)}\gamma_1^{(2)} & \gamma_2^{(2)} e_{150}^{(2)} & \gamma_2^{(2)} q_{150}^{(2)} \\ 0 & \gamma_2^{(2)} \varepsilon_{110}^{(2)} & \gamma_2^{(2)} d_{110}^{(2)} \\ 0 & \gamma_2^{(2)} d_{110}^{(2)} & \gamma_2^{(2)} \mu_{110}^{(2)} \end{bmatrix}$$

$$[\mathbf{X}_5] = [\mathbf{X}_1] - [\mathbf{X}_2][\mathbf{X}_4]^{-1}[\mathbf{X}_3]$$

$$[\mathbf{X}_6]=\begin{bmatrix}-\mu_0^{(1)}\gamma_1^{(1)} & -\gamma_2^{(1)}e_{150}^{(1)} & -\gamma_2^{(1)}q_{150}^{(1)}\\ 0 & \gamma_2^{(1)}\varepsilon_{110}^{(1)} & \gamma_2^{(1)}d_{110}^{(1)}\\ 0 & \gamma_2^{(1)}d_{110}^{(1)} & \gamma_2^{(1)}\mu_{110}^{(1)}\end{bmatrix}$$

$$[\mathbf{X}_7]=\begin{bmatrix}x_{11}(s) & x_{12}(s) & x_{13}(s)\\ x_{21}(s) & x_{22}(s) & x_{23}(s)\\ x_{31}(s) & x_{32}(s) & x_{33}(s)\end{bmatrix}=[\mathbf{X}_6][\mathbf{X}_5]^{-1}$$

$$g_1(s)=x_{11}(s),\quad g_2(s)=x_{21}(s),\quad g_3(s)=x_{31}(s)$$

The constants of β_1, β_2, and β_3 can be obtained by the operation of the following matrixes

$$[\mathbf{Y}_3]=\begin{bmatrix}\mu_0^{(1)} & e_{150}^{(1)} & q_{150}^{(1)}\\ 0 & \varepsilon_{110}^{(1)} & d_{110}^{(1)}\\ 0 & d_{110}^{(1)} & \mu_{110}^{(1)}\end{bmatrix}$$

$$[\mathbf{Y}_4]=\begin{bmatrix}\mu_0^{(2)} & e_{150}^{(2)} & q_{150}^{(2)}\\ 0 & \varepsilon_{110}^{(2)} & d_{110}^{(2)}\\ 0 & d_{110}^{(2)} & \mu_{110}^{(2)}\end{bmatrix}$$

$$[\mathbf{Y}_5]=[\mathbf{X}_1]-[\mathbf{X}_2][\mathbf{Y}_4]^{-1}[\mathbf{Y}_3]$$

$$[\mathbf{Y}_6]=\begin{bmatrix}-\mu_0^{(1)} & -e_{150}^{(1)} & -q_{150}^{(1)}\\ 0 & \varepsilon_{110}^{(1)} & d_{110}^{(1)}\\ 0 & d_{110}^{(1)} & \mu_{110}^{(1)}\end{bmatrix}$$

$$[\mathbf{Y}_7]=\begin{bmatrix}y_{11} & y_{12} & y_{13}\\ y_{21} & y_{22} & y_{23}\\ y_{31} & y_{32} & y_{33}\end{bmatrix}=[\mathbf{Y}_6][\mathbf{Y}_5]^{-1}$$

$$\beta_1=y_{11},\quad \beta_2=y_{21},\quad \beta_3=y_{31}$$

APPENDIX 3

From the relationships[30]

$$\int_0^\infty \frac{1}{s}J_n(sa)\sin(bs)\mathrm{d}s=\begin{cases}\dfrac{\sin[n\sin^{-1}(b/a)]}{n}, & a>b\\[2mm] \dfrac{a^n\sin(n\pi/2)}{n[b+\sqrt{b^2-a^2}]^n}, & a<b\end{cases}\tag{45}$$

$$\int_0^\infty \frac{1}{s}J_n(sa)\cos(bs)\mathrm{d}s=\begin{cases}\dfrac{\cos[n\sin^{-1}(b/a)]}{n}, & a>b\\[2mm] \dfrac{a^n\cos(n\pi/2)}{n[b+\sqrt{b^2-a^2}]^n}, & a<b\end{cases}\tag{46}$$

the semi-infinite integrals in equation (32) can be modified as

$$\begin{aligned}&\int_0^\infty \frac{1}{s}\left[\beta_1+\left(\frac{g_1(s)}{s}-\beta_1\right)\right]J_{n+1}\left(s\frac{1-b}{2}\right)\\ &\quad\times\cos\left(s\frac{1+b}{2}\right)\sin(sx)\mathrm{d}s\\ &=\frac{\beta_1}{2(n+1)}\\ &\quad\times\left\{\frac{((1-b)/2)^{n+1}\sin((n+1)\pi/2)}{\{x+(1+b)/2+\sqrt{(x+(1+b)/2)^2-((1-b)/2)^2}\}^{n+1}}\right.\\ &\quad\left.-\sin\left[(n+1)\sin^{-1}\left(\frac{1+b-2x}{1-b}\right)\right]\right\}\\ &\quad+\int_0^\infty \frac{1}{s}\left[\frac{g_1(s)}{s}-\beta_1\right]J_{n+1}\left(s\frac{1-b}{2}\right)\\ &\quad\times\cos\left(s\frac{1+b}{2}\right)\sin(sx)\mathrm{d}s\end{aligned}\tag{47}$$

$$\begin{aligned}&\int_0^\infty \frac{1}{s}\left[\beta_1+\left(\frac{g_1(s)}{s}-\beta_1\right)\right]J_{n+1}\left(s\frac{1-b}{2}\right)\\ &\quad\times\sin\left(s\frac{1+b}{2}\right)\sin(sx)\mathrm{d}s\\ &=\frac{\beta_1}{2(n+1)}\left\{\cos\left[(n+1)\sin^{-1}\left(\frac{1+b-2x}{1-b}\right)\right]\right.\\ &\quad\left.-\frac{((1-b)/2)^{n+1}\cos((n+1)\pi/2)}{\{x+(1+b)/2+\sqrt{(x+(1+b)/2)^2-((1-b)/2)^2}\}^{n+1}}\right\}\\ &\quad+\int_0^\infty \frac{1}{s}\left[\frac{g_1(s)}{s}-\beta_1\right]J_{n+1}\left(s\frac{1-b}{2}\right)\\ &\quad\times\sin\left(s\frac{1+b}{2}\right)\sin(sx)\mathrm{d}s\end{aligned}$$

It can be seen that the integrands in the right end of equations (47) and (48) tend rapidly to zero.

APPENDIX 4

For brevity, equation (32) can be rewritten as

$$\sum_{n=0}^{\infty}b_nE_n(x)=U(x),\qquad b\leqslant x\leqslant 1\tag{49}$$

where $E_n(x)$ and $U(x)$ are known functions and coefficients b_n are unknown and will be determined. A set of functions $P_n(x)$, which satisfies the orthogonality conditions

$$\int_b^1 P_m(x)P_n(x)\mathrm{d}x=N_n\delta_{mn},\qquad N_n=\int_b^1 P_n^2(x)\mathrm{d}x\tag{50}$$

can be constructed from the function, $E_n(x)$, such that

$$P_n(x) = \sum_{i=0}^{n} \frac{M_{in}}{M_{nn}} E_i(x) \tag{51}$$

where M_{ij} is the cofactor of the element d_{ij} of $\mathbf{D}_n$, which is defined as

$$\mathbf{D}_n = \begin{bmatrix} d_{00}, d_{01}, d_{02}, \ldots, d_{0n} \\ d_{10}, d_{11}, d_{12}, \ldots, d_{1n} \\ d_{20}, d_{21}, d_{22}, \ldots, d_{2n} \\ \cdots\cdots\cdots\cdots\cdots\cdots \\ \cdots\cdots\cdots\cdots\cdots\cdots \\ \cdots\cdots\cdots\cdots\cdots\cdots \\ d_{n0}, d_{n1}, d_{n2}, \cdots, d_{nn} \end{bmatrix}$$

$$d_{ij} = \int_b^1 E_i(x) E_j(x) \mathrm{d}x \tag{52}$$

Using equations (49) to (52), it can be obtained

$$b_n = \sum_{j=n}^{\infty} q_j \frac{M_{nj}}{M_{jj}}, \quad q_j = \frac{1}{N_j} \int_b^1 U(x) P_j(x) \mathrm{d}x \tag{53}$$

APPENDIX 5

$$\cos\left(s\frac{1+b}{2}\right)\cos(sx) = \frac{1}{2}\left\{\cos\left[s\left(\frac{1+b}{2} - x\right)\right] + \cos\left[s\left(\frac{1+b}{2} + x\right)\right]\right\}$$

$$\sin\left(s\frac{1+b}{2}\right)\cos(sx) = \frac{1}{2}\left\{\sin\left[s\left(\frac{1+b}{2} - x\right)\right] + \sin\left[s\left(\frac{1+b}{2} + x\right)\right]\right\}$$

$$\int_0^\infty J_n(sa)\cos(bs)\mathrm{d}s = \begin{cases} \dfrac{\cos[n\sin^{-1}(b/a)]}{\sqrt{a^2-b^2}}, & a > b \\ -\dfrac{a^n \sin(n\pi/2)}{\sqrt{b^2-a^2}[b+\sqrt{b^2-a^2}]^n}, & b > a \end{cases}$$

$$\int_0^\infty J_n(sa)\sin(bs)\mathrm{d}s = \begin{cases} \dfrac{\sin[n\sin^{-1}(b/a)]}{\sqrt{a^2-b^2}}, & a > b \\ \dfrac{a^n \cos(n\pi/2)}{\sqrt{b^2-a^2}[b+\sqrt{b^2-a^2}]^n}, & b > a \end{cases}$$